

Structural lubricity and fractures in liquid crystals

Weichao Zheng^{1,*}

¹*Department of Chemistry, Physical and Theoretical Chemistry Laboratory, University of Oxford, Oxford OX1 3QZ, United Kingdom*

Structural superlubricity, one of the most important concepts in modern tribology, has attracted lots of interest in both fundamental research and practical applications. However, despite promising theoretical models, such as the Prandtl-Tomlinson and Frenkel-Kontorova models, and great success in structural lubricant experiments with two-dimensional materials and colloids, these models have not been directly tested. Here, with the cholesteric liquid crystals confined under the Surface Force Balance, we measure the surface torque during rotational friction, and the molecular rotation from the commensurate to incommensurate configuration, at the onset of structural lubricity. Furthermore, by changing the surface potential, the Aubry transition is confirmed. The results agree well with the description by a modified three-dimensional version of the above models and provide molecular evidence for rupture nucleation during static friction. Our study bridges the gap between theories and experiments, and reinforces the connection between friction and fracture.

1 Introduction

One of the 125 questions [1] published in the *Science* journal in 2021 is how to measure interfacial phenomena at the microscale. For the interface between solids and solids, contact mechanics have been well-established. However, friction, which dates back to research five centuries ago, has not been well understood due to the multiple contacts at the nanoscale and the complicated dynamics involving physical interactions and chemical reactions [2,3].

Two significant signs of progress in the understanding of stick-slip motions have been made in the past decades. First, the experimental verification [4] of structural superlubricity with two-dimensional (2D) materials manifests the success of the one-dimensional (1D) Prandtl-Tomlinson (PT) and Frenkel-Kontorova (FK) models [5-7] that led to the development of the superlubric theory [8,9]. Another prediction based on the FK model, i.e., the Aubry transition [10], has also been observed in 1D cold ions [11] and 2D colloidal lattices [12]. However, the direct experimental testing of these two models has not been accomplished for several decades [13]. Second, the paradigm using brittle fracture theory [14] was developed and experimentally confirmed to describe the onset of kinetic friction from the static friction that had previously been described with the static friction coefficient. However, the mechanism of rupture nucleation during static friction at the microscopic level is still unclear [14,15]. The above puzzles are due to the difficulties of experimental characterization at the atomic interface.

Similarly, the interface plays a big role in the viscoelastic behavior of liquid crystals. Some historical puzzles, such as the discontinuous cholesteric-nematic transition [16] and permeative flows [17], have been ascribed to the boundary conditions. Recently, we studied [16] cholesteric mechanics with different surface anchoring strengths under the confinement of the Surface Force Balance (Fig. 1a). During the mechanical winding of cholesterics, three regimes, including constrained, stick-slip, and sliding-slip, were observed and explained with the balance of twist elastic torque and frictional surface torque [16]. Furthermore, we proposed [17] that the previous measurement of anomalous viscosity of cholesterics in the capillary is, in fact, the twist elasticity resulting from the confinement with a rather small Ericksen number. In other words, liquid crystals are elastic solids at small scales. In the present work, we interpret the slip behaviors

at the critical surface torque under mechanical winding as the reduction of friction by rotating liquid crystal molecules from the commensurate, namely the easy axis, to the incommensurate configuration, forming structural lubricity (Fig. 1b). The corrugated surface potential on the muscovite mica works like a grooved surface [18,19] to align molecules. At the easy axis, molecules lie on the commensurate position of grooves to minimize the twist distortion. While under stress, molecules rotate gradually to an incommensurate position with a maximum angle $\pi/2$ to the easy axis. With the decay of anchoring strength, it is easier to reach the incommensurate configuration, undergoing the Aubry transition. On the other hand, the rotation of molecules is the signature of rupture nucleation resulting in the propagation of rupture fronts until the slip occurs. Therefore, we consolidate the paradigm that static friction is interfacial rupture [14] and is indeed dynamic [20,21]. Finally, the relationship between dislocations and cracks is discussed.

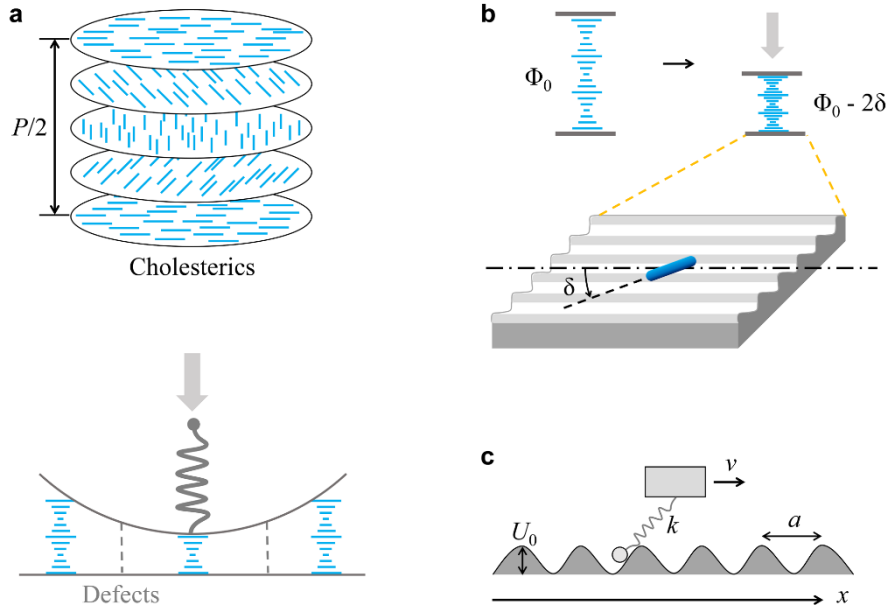


Fig. 1 Mechanical winding of cholesterics. (a) Schematic diagram of cholesterics under the confinement of crossed cylinders (front view), where $P = 244$ nm is the pitch. (b) The deviation of molecules from the easy axis under stress, where Φ_0 is the original twist angle, and δ is the deviated angle. The dot-dash line is the easy axis on the potential energy surface. (c) The Prandtl-Tomlinson model, $\frac{1}{2}U_0$ and a are the amplitude and periodicity of the surface potential, respectively, k is the spring constant, and v is the velocity along the x -axis.

2 Rotational friction and structural lubricity

In the Surface Force Balance (SFB), the surfaces are made of muscovite mica with atomic smoothness, and the interaction between the surfaces and cholesterics is not as strong as chemical bonds. As a result, the liquid crystal molecules rotate both in the bulk and on the surface to minimize the free energy under stress (Fig. 1b). The free energy per unit area G as a sum of the anchoring energy (one surface) and twist elastic energy by ignoring the dislocation energy is written as [16],

$$G = \frac{1}{2}W\delta^2 + \frac{1}{2}K_{22}\left(\frac{\Phi}{D} - q_0\right)^2D \quad (1)$$

where δ is the deviated angle of molecules to the easy axis, W is the anchoring strength, $K_{22} = 6$ pN is the twist elastic

energy, Φ is the total twist angle, D is the smallest surface separation between two crossed cylinders, and q_0 is the molecular rotation rate of cholesterics at relaxation. With strong anchoring strength, twist angle $\Phi = \Phi_0 - 2\delta \approx \Phi_0 = q_0 D_0$ keeps the relaxed twist angle Φ_0 at the original distance D_0 , thus,

$$G = \frac{1}{2} W \left(\frac{\Phi_0 - \Phi}{2} \right)^2 + \frac{1}{2} K_{22} q_0^2 \frac{(D_0 - D)^2}{D} \quad (2)$$

The form in Equation 1 is widely used in the liquid crystal community, sometimes with different expressions in the anchoring energy [22,23]. In fact, this form is a modified three-dimensional (3D) version of the PT model (Fig. 1c) below or the FK model with a quasi-static motion,

$$U(x, t) = \frac{1}{2} U_0 \cos\left(\frac{2\pi}{a} x\right) + \frac{1}{2} k(x - vt)^2 \quad (3)$$

where U is the free energy, $\frac{1}{2} U_0$ and a are the amplitude and periodicity of the surface potential respectively, k is the spring constant, v is the velocity along the x axis, and t is the time.

The rotational friction in cholesterics under confinement is a balance of the twist elastic torque Γ_e and the frictional anchoring torque Γ_a , by differentiating Equation 1 with respect to the twist angle Φ , while ignoring the viscous torque with a strong anchoring limit,

$$\Gamma_e = K_{22} \left(\frac{\Phi}{D} - q_0 \right) = \Gamma_a = \frac{1}{2} W \frac{\Phi_0 - \Phi}{2} \quad (4)$$

$$K_{22} q_0 \left(\frac{D_0}{D} - 1 \right) = \frac{1}{2} W \frac{\Phi_0 - \Phi}{2} \quad (5)$$

During surface compression at a speed smaller than 4 nm/s, cholesterics underwent an elastic response and then yielded when reaching the maximum surface torque, resulting in a surface jumping event (Fig. 2, a and b). Fig. 2c shows that indeed the compression ratio at the critical jumping distance remains almost constant at about 0.2-0.4, with different half-pitch layers of cholesterics. If the threshold of the critical surface torque Γ_c at the critical jumping distance D_c is assumed [16],

$$D_c = \frac{D_0 - \frac{4\Gamma_c}{q_0 W}}{1 + \frac{\Gamma_c}{K_{22} q_0}} \quad (6)$$

From the fitting line in Fig. 2d, the critical torque $\Gamma_c \approx 0.22$ mN/m and anchoring strength $W \approx 0.27$ mN/m can be calculated using Equation 6 and the pitch $P = 244$ nm. Meanwhile, the deviated angle $\delta \approx 0.52\pi$ is obtained using Equation 4, which is consistent with the previous result [16], i.e., $\delta \approx 0.49\pi$. The deviation of molecules by around $\pi/2$ from the easy axis is a signature of structural lubricity at the maximum incommensurate configuration. Therefore, the barrier to have a slip is the activation energy required to get structural lubricity.

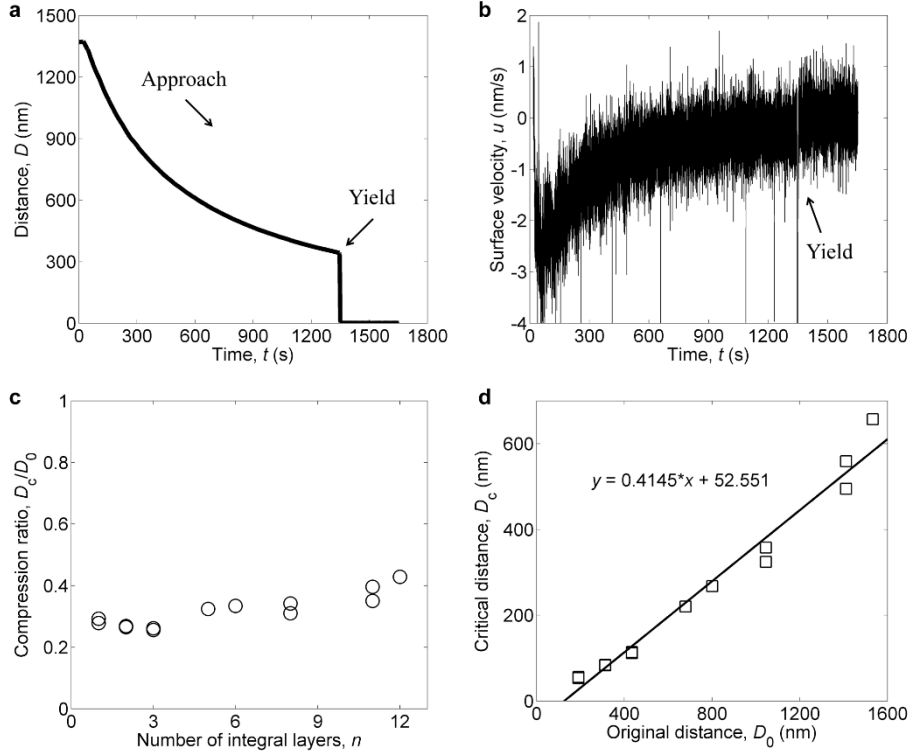


Fig. 2 Slippage of cholesterics at the incommensurate position. (a) The elastic response and yield of cholesterics during the surface approach. (b) Corresponding surface velocity. (c) The compression ratio of cholesterics with various layers in the jumping events. (d) The critical yield distance as a function of the original distance. The line is the linear fit.

3 Aubry transition

In the PT model, a dimensionless parameter η is calculated to predict the stick-slip behaviors, which is the ratio between the stiffness of the surface potential and the spring [3,24],

$$\eta = \frac{2\pi^2 U_0}{ka^2} \quad (7)$$

By analogy, the parameter η_f based on Equation 2 is also calculated,

$$\eta_f = \frac{W}{k_{chl}} \quad (8)$$

where $k_{chl} = K_{22}q$ is the spring constant of the cholesterics.

With time evolution, probably due to the adsorption of water that smoothens the corrugation of the surface potential, the anchoring strength decreases. As a result, the transition goes from the constrained regime (initially $\eta_f > 1$), stick-slip, to the sliding-slip regime ($\eta_f < 1$) [16], which is the Aubry transition by decreasing the surface potential. In other words, the stress-induced incommensurate status changes from a pinned status to a continuous transition layer by layer with a smaller corrugation of surface potential. On the other hand, the jump process (i.e., kinetic friction) is continuous in the constrained regime while it is discontinuous in the stick-slip regime [16], which is another Aubry transition by increasing the spring constant (i.e., strain-stiffening) of cholesterics with larger compression ratio [17]. With the stiffer spring constant of cholesterics, there is not enough time for the slower molecules to recover from the incommensurate configuration during

slip to the commensurate configuration, such that the structural lubricity continues.

4 Fractures in cholesterics

Under compression, cholesterics elastically deform and finally yield at a critical friction torque, which is also a typical fracture behavior. The rotation of molecules from the commensurate to the 0.52π incommensurate configuration during mechanical winding is a signature of rupture nucleation that cannot be observed in a solid interface with stiff materials. Thanks to the weak interaction between liquid crystal molecules and the mica surface, the anchoring deviation is quite obvious, commonly observed under a polarized microscope in the liquid crystal community [25-27]. However, without high mechanical stress, no large azimuthal deviations can be detected. With a small deviation, it is difficult to test the exact form of the anchoring energy. From what we obtained above, the parabolic potential was valid at a large deviation; however, the Rapini-Papoula potential failed [16].

With fracture mechanics, it is easier to explain the differences in the distance profile and surface velocity, and the hysteresis on force profile and twist transition during the approach and retraction of surfaces (Fig. 3, c to f). During retraction, there was a jump-out event because of the strong adhesion at the contact position (Fig. 3, c to e). Cholesteric layers behave like elastic solids with a small Ericksen number. The innermost dislocation defect serving as a crack breaks the neck of layers (Fig. 3a), which is analogous to the opening mode of fracture in a rod with cracks (Fig. 3b). Simultaneously, a new layer comes to fill the increased height (Fig. 3f). The neck-breaking and the slip-in are alternate layer-by-layer (Fig. 3f). This breakup is not the same as the break of a liquid jet due to the Plateau-Rayleigh instability [28]. By contrast, during the approach, defects move to a larger radius, such that they never become cracks, but the whole layers undergo a shear mode fracture encountering large fracture energy before yielding (Fig. 3, a to f). Under such circumstances, cholesterics behave like ceramics that resist compression but not tension.

The adhesion between two crossed cylinders or two spheres at contact during retraction has been proven to be the opening mode of fracture for decades [29]. We may also speculate that rolling friction is also the crack opening on one side that decreases the dissipated energy compared to the tearing mode of the normal stick-slip friction.

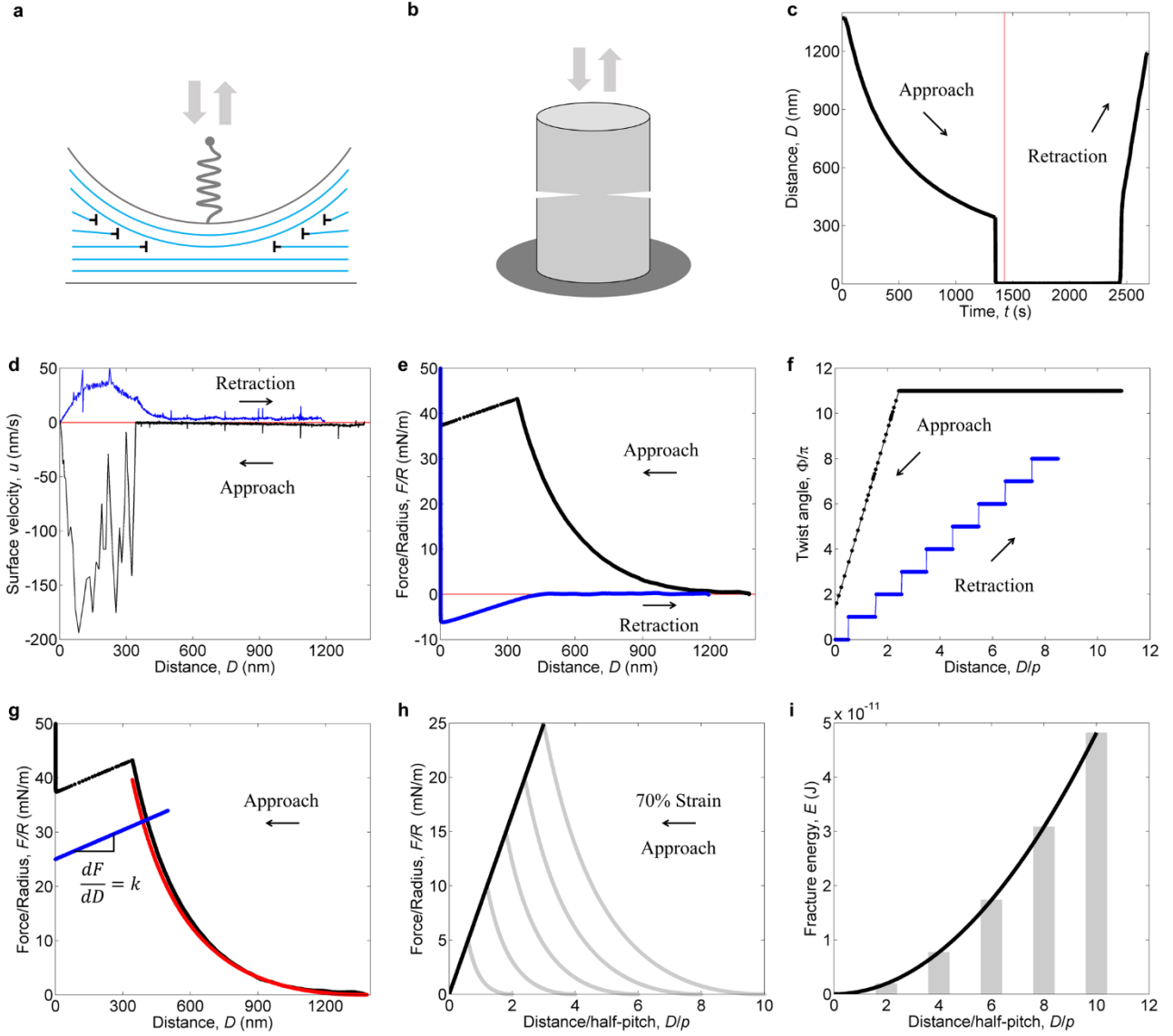


Fig. 3 Fractures in cholesterics. (a) Dislocations of cholesterics in the SFB. (b) A rod with two cracks. (c-f) The differences in the distance profile, surface velocity, force profile, and twist transition during approach and retraction. The red line in (c) separates the approach and retraction regimes. The non-integral layer has been deducted in (f). (g) The force profile of cholesterics during the surface approach. The red line is the theoretical fit using Equation 9. $R = 1$ cm is the radius of crossed cylinders. The blue line is the slope of the SFB spring with a spring constant $k = 179$ N/m. (h) The force profiles up to 70% strain with different layers calculated by Equation 9. The black line is the linear fit of the maximum forces. (i) The fracture energy calculated by integrating the force profiles with respect to the strain in (h). The black line is the parabolic fit of the fracture energy. The symbol p is the half-pitch.

With the strong anchoring assumption, the anchoring energy is negligible compared to the twist elastic energy. Thus, the elastic force with n layers is calculated by the second term on the right side of Equation 2 with Derjaguin approximation,

$$F = 2\pi R G^n = \pi R K_{22} q_0^2 \frac{(D_0^n - D)^2}{D} \quad (9)$$

The measured forces can be well fitted by the force calculation using Equation 9, confirming an elastic deformation (Fig.

3g). Fig. 3h shows that the forces generated by different layers with the same strain are different with a linear increase proportional to the number of layers. While the fracture energy calculated from these force profiles increases parabolically (Fig. 3i, which is different from the linear increase of elastic energy in normal springs with different lengths. The increase in fracture energy is consistent with a previous study [30] showing that lubricants increase the fracture energy since, in dry friction, the stiffness of the surface is quite large decreasing the stored energy.

5 Dislocation path

With fracture mechanics, it is easier to understand the formation of dislocation defects in the SFB and Grandjean-Cano wedge (Fig. 4). At a height equal to n integral layers, the cholesterics are relaxed. By contrast, integral cholesterics are compressed on the left side and stretched on the right side, i.e., $D_0 \pm \Delta D$ (Fig. 4b), which is more significant at small heights with relatively strong deformation. By increasing the heights, the layers are further stretched until a new layer is added to minimize the free energy. Therefore, with less intense deformation, the Burgers vector $b = \frac{1}{2}nP$ gradually increases at large distances [31,32]. In a more complex geometry with bumps and hollows (Fig. 4c), the dislocations automatically form an isoheight map. The dislocations are denser in bumps with larger heights compared to those in hollows. At large distances, thicker dislocation lines may be observed due to the increase of the Burgers vector. The geometry of confinement may provide a method to design defect networks [33] with different topological structures.

When the anchoring strength is strong, the disordered dislocations will be repelled to the bisector of the confinement, while with weak anchoring strength, the dislocations will be attracted to the surface [34]. This behavior provides a method to engineer the distribution of dislocations in materials. Furthermore, the paths of disordered dislocations are analogous to the crack paths designed on curved surfaces [35,36]. In other words, the disordered dislocations visualize the region with higher stress intensity [35,36], and the order parameter in liquid crystals serves as a single variable to predict how cracks propagate in a complex geometry. Meanwhile, the thickness of the dislocation line is associated with the levels of stress intensity.

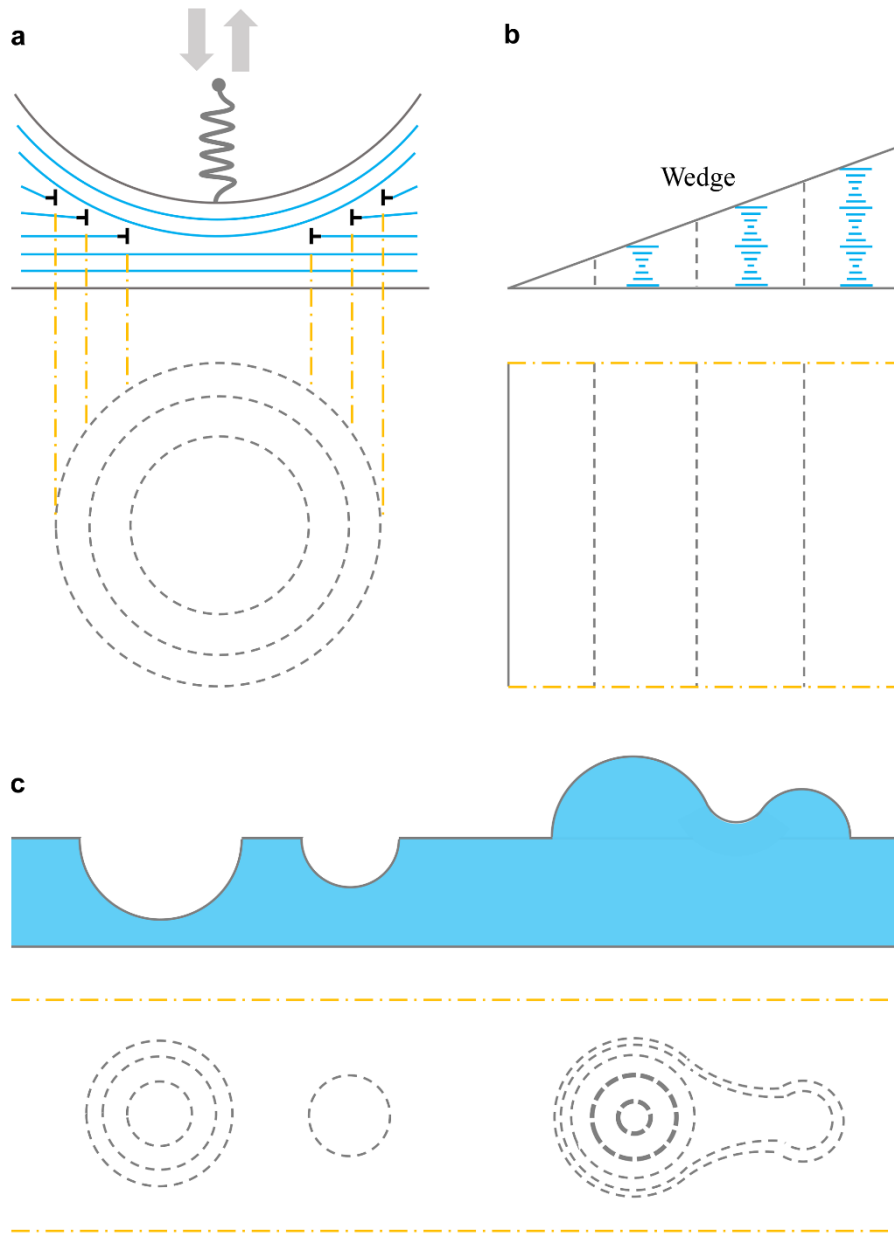


Fig. 4 Dislocations in different geometries. Front-view and top-view of cholesteric dislocations in (a) the SFB, (b) the Grandjean-Cano wedge, and (c) a geometry with bumps and hollows. The dashed lines represent dislocations, the dot-dashed lines are guidelines, and the thick dashed lines in (c) are thick dislocations.

6 Discussions

Many concepts in liquid crystals are borrowed from the crystalline community, such as dislocation and piezoelectricity. Conversely, the concept of disclination, which was developed in liquid crystals, has been used later in crystals [37]. Despite the well-developed elastic energy theory, liquid crystals are considered as fluids [38]. Therefore, fracture mechanics has rarely been used to describe liquid crystal behaviors. Even the concept of surface torque is rarely used in the liquid crystal community [16]. Our previous study [17] highlighted the importance of elasticity with strong surface anchoring under confinement. This work further underlines the friction and fractures in liquid crystals, which promotes the understanding of structural lubricity and interfacial ruptures in crystals.

Although the exact form of the anchoring potential is not proven, it is reasonable to use the parabolic potential [22], since the elastic energy of liquid crystals is based on Hooke's law. The twist interaction of molecules with the surface is similar to the elastic interaction between cholesteric molecules. In fact, the anchoring potential could be verified by measuring both the surface separation and the deviated angle, simultaneously. For example, the newly developed μ SFA [39] can be mounted into the polarized microscope for this purpose.

If we compare the static rotational friction with the dry sliding friction ruled by the Coulomb-Amontons laws, it is apparent to see that, firstly, the surface torque is independent of the contact area (Equation 4). Secondly, the surface torque is independent of the approaching speed outside the viscous regime [16]. Thirdly, the surface torque is proportional to the deviated angle (Equation 4) rather than the normal load. However, in Coulomb-Amontons laws, the normal load also could be described by the elastic deformation of the contact area through Hooke's law, which, therefore, is proportional to the strain. In other words, the traditional sliding friction is proportional to the strain.

It has been shown [40] that the maximum dissipated energy during friction is equal to the corrugation of the potential energy surface, which seems to be the first term of Equation 1 if the second term did not dissipate as phonons. For cholesterics, the rotation of molecules along the helical axis also causes piezoelectricity [41], which needs to be taken into account as electronic dissipation. In the stick-slip regime, apart from the dissipated heat, residual energy is also stored in the rest layers until all the layers are squeezed out.

There has been a lasting debate [42,43] on the mechanism of stick-slip motions during molecular friction. Three scenarios, including one-layer or whole-layers melting and interlayer slip, have been proposed [42]. It is difficult to distinguish the melting and the slip when the heat dissipation from the fracture energy is high enough to melt molecular layers or cause wear during stick-slip. However, from the results of this work, it may be more favorable for the scenario of interlayer slip [43,44], which is also a signature of interfacial ruptures at the molecular level.

7 Conclusions

We directly tested the PT and FK models with cholesterics under mechanical winding in the SFB. During rotational friction, liquid crystal molecules gradually rotated from the commensurate to incommensurate configuration with a balance of the twist elastic torque and the surface torque. With strong anchoring, molecules parabolically rotated 0.52π reaching the maximum incommensurate status and structural lubricity occurred. By either decreasing the surface potential or increasing the stiffness of cholesterics with fewer layers, the Aubry transition from constrained, stick-slip, to sliding-slip status was observed. Furthermore, the rotation of molecules is the signature of molecular rupture nucleation that cannot be easily observed in crystals, which leads to the explanation of the mechanical hysteresis during retraction and approach with different modes in fracture mechanics. Additionally, we showed that the dislocation path forms the isoheight map and provides guidance for the design of the crack path. This experiment provides a model system for studying friction with tunable surface potential, elastic constants as well as cholesteric pitch length by external stimuli, such as light, temperature, stress, dopants, and magnetic and electric fields. It may shed light on the understanding of surface anchoring, structural lubricity, shear thickening [45], glass transition, yield stress materials, and earthquakes.

Acknowledgment

W.Z. is very grateful to S. Perkin who suggested that the $\pi/2$ deviation of anchoring may be intrinsic. Some parts of this work have been discussed in the Ph.D. thesis titled "Optical and mechanical responses of liquid crystals under confinement (2020)". This research was supported by the European Research Council (Grant Nos. ERC-2015-StG-676861 and 674979-

NANOTRANS).

*zwhich@outlook.com

References

- [1] Science (2021).
- [2] Y. F. Mo, K. T. Turner, and I. Szlufarska, *Nature* **457**, 1116 (2009).
- [3] A. Vanossi, N. Manini, M. Urbakh, S. Zapperi, and E. Tosatti, *Rev. Mod. Phys.* **85**, 529 (2013).
- [4] M. Dienwiebel, G. S. Verhoeven, N. Pradeep, J. W. M. Frenken, J. A. Heimberg, and H. W. Zandbergen, *Phys. Rev. Lett.* **92** (2004).
- [5] L. Prandtl, *ZAMM-Journal of Applied Mathematics and Mechanics/Zeitschrift für Angewandte Mathematik und Mechanik* **8**, 85 (1928).
- [6] G. Tomlinson, *The London, Edinburgh, and Dublin philosophical magazine and journal of science* **7**, 905 (1929).
- [7] J. Frenkel and T. Kontorova, *Izv. Akad. Nauk, Ser. Fiz.* **1**, 137 (1939).
- [8] M. Hirano, K. Shinjo, R. Kaneko, and Y. Murata, *Phys. Rev. Lett.* **67**, 2642 (1991).
- [9] K. Shinjo and M. Hirano, *Surf Sci.* **283**, 473 (1993).
- [10] M. Peyrard and S. Aubry, *Journal of Physics C-Solid State Physics* **16**, 1593 (1983).
- [11] A. Bylinskii, D. Gangloff, I. Counts, and V. Vuletic, *Nat. Mater.* **15**, 717 (2016).
- [12] T. Brazda, A. Silva, N. Manini, A. Vanossi, R. Guerra, E. Tosatti, and C. Bechinger, *Phys. Rev. X* **8** (2018).
- [13] A. Vanossi, C. Bechinger, and M. Urbakh, *Nat. Commun.* **11** (2020).
- [14] I. Svetlizky, E. Bayart, and J. Fineberg, *Annu. Rev. Condens. Matter Phys.* **10**, 253 (2019).
- [15] S. Gvirtzman and J. Fineberg, *Journal of Geophysical Research-Solid Earth* **128** (2023).
- [16] W. C. Zheng, In Preparation.
- [17] W. C. Zheng, In Preparation.
- [18] D. W. Berreman, *Phys. Rev. Lett.* **28**, 1683 (1972).
- [19] D. W. Berreman, *Mol. Cryst. Liq. Cryst.* **23**, 215 (1973).
- [20] Z. P. Yang, H. P. Zhang, and M. Marder, *PNAS* **105**, 13264 (2008).
- [21] M. H. Muser, *PNAS* **105**, 13187 (2008).
- [22] P.-G. De Gennes and J. Prost, *The physics of liquid crystals* (Clarendon Press, Oxford, 1993), 2nd ed edn., Oxford science publications.
- [23] A. Rapini and M. Papoular, *Le Journal de Physique Colloques* **30**, C4 (1969).
- [24] A. Socoliuc, R. Bennowitz, E. Gnecco, and E. Meyer, *Phys. Rev. Lett.* **92** (2004).
- [25] G. Barbero, N. Madhusudana, J. Paliarne, and G. Durand, *Phys. Lett. A* **103**, 385 (1984).
- [26] M. Jiang, Z. Wang, R. Sun, K. Ma, R. M. R. Ma, and X. H. X. Huang, *Jpn. J. Appl. Phys.* **33**, L1242 (1994).
- [27] D. V. Shmeliova and V. A. Belyakov, *Mol. Cryst. Liq. Cryst.* **646**, 160 (2017).
- [28] D. R. Link, S. L. Anna, D. A. Weitz, and H. A. Stone, *Phys. Rev. Lett.* **92** (2004).
- [29] K. L. Johnson, *Langmuir* **12**, 4510 (1996).
- [30] E. Bayart, I. Svetlizky, and J. Fineberg, *Phys. Rev. Lett.* **116** (2016).
- [31] J. C. Geminard, C. Laroche, and P. Oswald, *Phys. Rev. E* **58**, 5923 (1998).
- [32] I. I. Smalyukh and O. D. Lavrentovich, *Phys. Rev. E* **66**, 051703 (2002).

- [33] M. F. Wang, Y. N. Li, and H. Yokoyama, *Nat. Commun.* **8** (2017).
- [34] I. I. Smalyukh and O. D. Lavrentovich, *Phys. Rev. Lett.* **90**, 085503 (2003).
- [35] K. Kamrin, *Nat. Mater.* **16**, 8 (2017).
- [36] N. P. Mitchell, V. Koning, V. Vitelli, and W. T. M. Irvine, *Nat. Mater.* **16**, 89 (2017).
- [37] J. Hirth, *Metall. Trans. A* **16**, 2085 (1985).
- [38] D. Marenduzzo, E. Orlandini, and J. M. Yeomans, *Phys. Rev. Lett.* **92**, 188301 (2004).
- [39] K. Kristiansen, J. S. H. Donaldson, Z. J. Berkson, and e. al., arXiv preprint (2019).
- [40] M. Wolloch, G. Levita, P. Restuccia, and M. C. Righi, *Phys. Rev. Lett.* **121** (2018).
- [41] C. C. Chang, L. C. Chien, and R. B. Meyer, *Phys. Rev. E* **55**, 534 (1997).
- [42] J. N. Israelachvili, *Intermolecular and surface forces* (Academic press, 2011).
- [43] I. Rosenhek-Goldian, N. Kampf, A. Yeredor, and J. Klein, *PNAS* **112**, 7117 (2015).
- [44] P. A. Thompson and M. O. Robbins, *Phys. Rev. A* **41**, 6830 (1990).
- [45] M. Wyart and M. E. Cates, *Phys. Rev. Lett.* **112** (2014).